Tribology International 141 (2020) 105906

Contents lists available at ScienceDirect

Tribology International

journal homepage: www.elsevier.com/locate/triboint

Study of the mechanism of friction on functionally active tribological Polyvinyl Chloride (PVC) – Aggregate composite surfaces

Konstantinos Giannoukos, Konstantinos Salonitis*

Manufacturing Theme, Cranfield University, Cranfield, MK43 0AL, United Kingdom

ARTICLE INFO

Keywords:
PVC
SiC
Tribology
High friction surfaces

ABSTRACT

Polyvinyl Chloride (PVC) based surfaces present a relatively low coefficient of friction (COF), but this can be improved if silicon carbide (SiC) is dispersed on the surface. In the present paper an experimental investigation is presented for assessing the efficiency of the use of SiC aggregates for this purpose. FTIR and DSC methods were used for assessing the curing of the composite surfaces. Optical microscopy was used for assessing the geometrical characteristics of the SiC aggregates. The surface roughness of the composite surfaces was also measured and corelated to COF. The COF was measured using scratch test and an industry specific test. The friction mechanisms due to the use of the aggregates are discussed.

1. Introduction

The understanding of the impact of surface topography on the coefficient of friction (COF) is important for the design of new tribological surfaces with the desired properties [1]. In fact the field entitled "surface texturing" accounts for more than 400 papers since 1965 [2] and has created new dimensions in controlling friction mimicking natural analogues [3]. COF of composite polymeric surfaces is of special interest [4] as they are used in everyday surfaces from trains and buses to hospitals and schools [5,6]. In those applications, the highest achievable COF is essential for the safe human locomotion [7] and thus a rigorous understanding of the friction mechanisms allow for a better control of the manufacturing process and the final frictional behaviour [8]. New directions in tribology that demand the use of low [9] or high temperatures [10], require the multiscale understanding of tribology [11] and most importantly the understanding of the origins of friction for low modulus materials [12].

COF is attributed in the case of polymers to two main mechanisms; friction and adhesion [13]. The tribology of polymers, being in most cases composites of a main matrix with fillers and additives such as coloring agents [14], flame retardants [15] and other additives providing a wide range of functions [16], was found to depend strongly on the chemical composition of the final polymeric composite [17]. The friction forces of polymers, likewise to metals and ceramics, are explained from the contacting asperities theory and their plastic deformation during friction [18]. Many studies have focused on single asperity models for understanding the contact area and stresses between a counterface and a polymer [19] and some have successfully generated numerical models for predicting the COF [20]. However the problem of friction mechanism was proved to include multiple contacting asperities that deform elastically and plastically [21].

Despite the impact of the different hardness of polymers to ceramics and metals on the COF [22], the main friction due to the mechanical interlocking [23] is separated here from the adhesive/plastic part of friction. In the case of mechanical friction, the friction forces are applied on the asperities generated by the surface topography that is controlled on the one hand by the surface finish [24], and on the other hand by the molecular packing [25]. The so-called tribological tuning of a surface regarding mechanical friction and adhesion has been investigated for PDMS and was proved to be achievable at surfaces from the level of microscale using ordered surface patterns [26]. In addition, recent research on polymer-steel systems has revealed the importance of the testing conditions for the friction and the crucial impact of load and designed polymer surface for the understanding of the controlling factor for friction [27]. The tuning of a polymeric surface as a tribological surface has been shown to happen at the stage of manufacturing like in polymer brush polymers with controlled wetting properties and thus lubrication performance [28]. Macroscopically, the asperities for the mechanical interlocking can be from coarse aggregates to very fine particles and their microstructure has been found to control the COF for asphalt mixtures [29]. Despite the plethora of research in the governing factors of friction in hard materials like asphalt [30], ceramics [31] and metals [32], little is known for the friction in polymers when aggregates are added in order to achieve a certain COF.

* Corresponding author.
E-mail address: k.salonitis@cranfield.ac.uk (K. Salonitis).

https://doi.org/10.1016/j.triboint.2019.105906
Received 28 April 2019; Received in revised form 13 August 2019; Accepted 15 August 2019
Available online 15 August 2019

Regarding the adhesion part of friction, the adhesion forces are due to the van der Waals forces [33], that occur in the temporary contact of two surfaces and are more evident in elastically deformed surfaces due to the higher contact surface areas [34]. The adhesion in polymers happens mainly due their compressible nature. When two polymeric surfaces are in stationary contact for a sufficient duration those forces increase leading to the definition of the static friction due to the absence of sliding [35]. The adhesive part of friction can be expressed either by elastic deformation and recovery [36] or by plastic deformation and removal of material [13]. The adhesive control over friction is, in most cases, a strong phenomenon in flat surfaces or surfaces whose microstructures are brought into contact eliminating elastically or plastically the various asperities [37]. Adhesion and mechanical friction have been found to be competitive phenomena and to depend on both the properties of the two contacting surfaces and the speed of sliding [38]. In the current study the adhesive forces of the sliding rubber of the British pendulum on the examined surfaces are not studied, but are explained in the concept of the leakage of liquid film between the contacting surfaces [39] when mechanical friction is deemed unable to explain the measured COF. That phenomenon, has been investigated previously [40], and has been found to be particularly associated with the class of polymer based surfaces that have altering "physical contact areas" both spatially and timely [41].

The aim of the present paper is the investigation of the impact of the presence and microstructure of the Silicon Carbide (SiC) aggregates on the COF for Polyvinyl Chloride (PVC) surfaces. The major topics discussed include be the correlation of the amount of SiC placed at the surface of the surfaces on the COF, the understanding of the main geometrical parameters that govern wet friction and finally the impact of the surface topography due to the variable quantities of SiC –incorporated at the surface of an elastic material-on the COF.

2. Methods and materials

2.1. Methods

The methods used to understand the impact of the different quantities of surface SiC on the COF are given below. First of all, chemical methods were used to assess the stability of the curing in the production of the PVC composite samples. Secondly, microscopic images were used to characterise the aggregates' geometrical parameters before and after incorporating the SiC aggregates at the surfaces of the samples. To continue with, surface roughness was measured to assess the topographical parameters of each surface and correlation with the geometrical parameters of the SiC aggregates. Finally, two tribological techniques were used to compare the COF as given from the British pendulum with the results from the scratch testing machine.

2.1.1. PVC chemistry

The chemistry of the PVC surfaces was examined in order to verify that the differences in the COF are due to the impact of the aggregates and not the differences in chemistry that would have resulted in different wetting properties [42]. Any difference in the wetting properties would have caused different behaviour of the thin water film [43] according to the squeeze film theory, altering the sliding of the rubber of the British pendulum and thus would not have allowed comparisons in friction due to the aggregates.

The curing of the PVC plastisol was measured by means of FTIR and DSC. The FTIR was used for the identification of the various molecular arrangements of the PVC based on the characteristic wavenumbers during the absorption of the infrared radiation. The model Spectrum One FT-IR Spectrometer from PerkinElmer was used from 4000 cm^{-1} to 650 cm^{-1} based on the major frequencies during IR absorption by PVC [44]. For each sample at least three positions were analysed away from the SiC aggregates and the identification of the characteristic wavenumbers was done using the automatic selection from the software supplied by PerkinElmer.

The DSC was undertaken using a DSC Q2000 unit by TA instruments in order to check that the degree of curing was the same for all the samples. The DSC analyses were done in a nitrogen atmosphere at a purging rate of 50 ml/min from 25°C to 200°C at a heating rate of 10°C.

2.1.2. Aggregates analysis

For the calculation of the impact of the aggregates' geometry on the COF, various parameters like aggregates number, circularity, aspect ratio and Feret number were measured with observation methods that allowed the statistical analysis of the random scattering of the aggregates.

2.1.2.1. Gravimetric method – Volumetric analysis of aggregates. The simplest way of measuring the aggregates number is by weighing pure PVC samples and compare that with the weight of PVC samples with dispersed SiC. The net weight (w_i) of the accumulated SiC aggregates can thus be calculated. The number of the particles a_i for each one of the samples i is calculated as per the following equation:

$$\alpha_i = \frac{w_i}{\left(\frac{4}{3}\pi r^3\right)\rho} \tag{1}$$

where: i is the sequence number of the samples with $i = 0$ corresponding to the PVC with no aggregates; a_i is the number of particles per sample; w_i is the weight of the aggregates per sample; $r$is the mean radius of the particles and ρ is the density of the SiC (g/cm^3). In this case with a_i is symbolized the total number of particles that can be placed on the surface with no or negligible penetration of the aggregates at the bulk volume of the PVC matrix.

2.1.2.2. Surface analysis. Alternatively, optical microscopy images can be used for the calculation of the number of surface aggregates and their geometrical parameters like circularity, roundness, Feret (minimum, maximum, average), aspect ratio and solidity. These geometrical variables were measured using the commercially available imaging processing software, ImageJ. The number of the

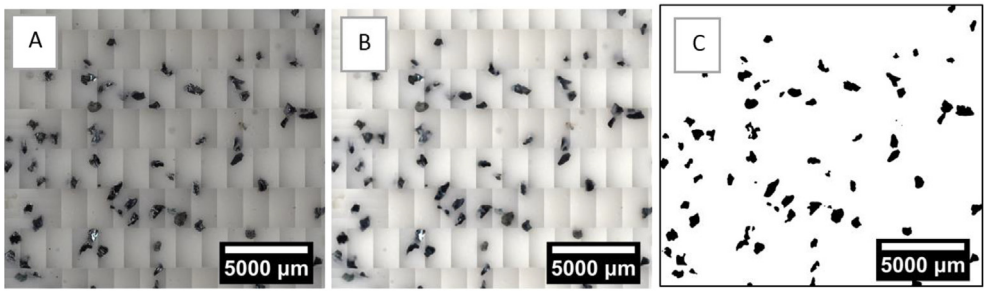

Fig. 1. The procedure for calculation of the number of aggregates using ImageJ. (A) The original image from the microscope; (B) the image corrected for the brightness, contrast and filtered for the unevenness of the grey level; (C) the final thresholded image for clear delineation of the aggregates from the PVC matrix.

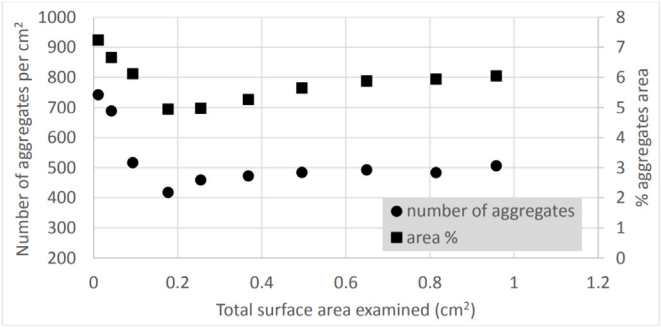

Fig. 2. Analysis of the surfaces for the detection of the representative surface area for the calculation of the true spatial density of the PVC – aggregate composite surfaces.

particles was calculated by the optical microscope used, which was a Hirox 3D Digital Microscope RH-2000.

Fig. 1-A shows an image taken with the microscope in the automatic 2D-tilling method in order to capture an area with the same, statistically, number of SiC aggregates per unit area. The tiling method was essential so as to capture an area big enough, that would give the same number of SiC aggregates per unit area irrespectively of the sampling area. Fig. 2 shows that the choice of an area 1 cm × 1 cm gives statistically constant number of SiC aggregates per unit area and constant % area, which is the percent of the area enclosed at the perimeter of the aggregate. That perimeter is in fact the interfacial zone between the part of the aggregate, which exceeds from the PVC matrix, and the PVC surface.

The confirmation of the number of the aggregates from the image analysis with the number from the automatic method of the microscope was essential for the validity of the geometrical parameters.

2.1.3. Roughness

The roughness of all the surfaces was measured as an indication of the topographical changes from the addition of the aggregates. For the measurement of the roughness a Mitutoyo Surftest SJ-310 Portable Surface Roughness Tester was used. The measurement of the roughness took place across lines of length 12.5 mm each for at least four different locations of the surface with the same content of aggregates. The roughness parameters tested were the centre mean average Ra, the ten point height average Rz, the total roughness at the extreme points of the roughness profile Rt and the Rsk and Rku that represent the skewness and kurtosis, respectively. For the roughness measurement the ISO protocol was used, that specified a sampling cut-off wavelength equal to 2.5 mm. That cut-off value was used since it was found to be more realistic since it appeared to have better correlation with the true roughness parameters [45].

2.1.4. Coefficient of friction (CoF)

2.1.4.1. British pendulum. The CoF was measured using two independent methods. The first one was the British pendulum device that allowed the measurement of a pendulum test value (PTV) and the calculation of the COF from an empirical equation as given by Ref. [46]. The calculation of the PTV is done via the sliding of a rubber slider of orthogonal shape, which upon sliding on a surface loses energy due to friction. That energy loss is transferred to a system of springs that adjust the position of an indicator in relation to that amount of lost energy due to the sliding. Two different sliders were used for the measurement of the PTV with shore A hardness 96 and 55. The conditioning of the sliders and the testing of the wet PTV was done in accordance with the relevant standard [47]. The main purpose of the two different sliders was to capture the impact of the different peak heights due to the aggregates on the CoF (see Fig. 3). In fact the a priori hypothesis for the contact behaviour of the two rubbers as proposed in Fig. 3, represents the real contact between asperities of a rubber substrate with a harder material [48]. The measurement of the PTV was done in wet conditions using tap water on the basis of the much better understanding of the frictional behaviour of a surface under wet conditions in comparison to the dry friction [49].

The use of wet conditions for the British pendulum was justified from the increased wear of both rubber sliders at dry conditions that was giving constantly changing BPN for the same surface. The sliders' wear was providing very deviant BPN as the aggregates spatial density increased, a fact well known in British pendulum testing in surfaces with coarse texture [50]. In most conditions wet friction is the most important area to focus due to increased accidents in wet conditions rather than dry [51].However, the multiple variables in the study of the sliding between two elastic surfaces especially in wet conditions [52] requires the generation of a great number of case studies that makes the need of understanding the inherent friction of the surface imperative using a counterface with no severe deformations like the scratches of the sliders. In the wet condition using the british pendulum, it is assumed the formation of a liquid film according to the squeeze film theory.

2.1.4.2. Single pass scratch test under constant load. For the second measurement of the COF, a single pass scratch test under constant load was implemented for normal loads 10 N, 20 N and 40 N. The measurement of the friction force for a travelling distance 40 mm allowed for the calculation of the COF by dividing the friction force to the normal load for each case. The linear velocity was 20 mm/min and the indenter a chrome steel ball with diameter 5 mm. For the scratch test the model ST30 was used supplied by Teer Coatings LTD. The test was conducted in dry conditions owning to the instrument's limitations. The use of a rubber ball at the size of the steel ball was deemed inappropriate due to on the one hand the severe wear of the rubber at that size, the difficulty of preparation of an ideally rubber ball (similarly to the ideal shape of the steel ball) and on the other hand the alteration of the instrument's preexisted list of sliders with known physical characteristics and calibration standards. The latter would have required the calibration of the rubber ball when sliding over standard surfaces [53] and the production of rubber balls according to the standard and certified procedure of production of the steel balls [54].

The use of a scratch testing using a different –non elastic-counterface meant that the measured COF was due to the measured surface alone. In other words, the COF using the steel ball was depended solely on the PVC surface and the density of the aggregates. The use of constantly increasing normal load in the scratch test would have caused inconsistencies due to the random position of the aggregates and the uncertainties for the homogeneity of the friction force at each aggregate. In fact the use of the scratch test under normal load allows the detection of any heterogeneity that could emanate from the mounting of an aggregate in the PVC matrix. The dry scratch test also prevented the existence of a non-uniform water film on the surface, and particularly around aggregates, a film with a thickness difficult to be controlled.

2.2. Materials

Nine PVC surfaces were prepared with different percentages of SiC aggregates (see Table 1).One surface contained no aggregates, as a reference sample, so as to measure the clear impact of the aggregates addition on the coefficient of friction. The target was to prepare the PVC surfaces with various surface coverage percentages of the aggregates, ideally from a small percent (*e.g.* 2–3% per area) to full coverage of the surface (*e.g.* 95% per area). The main hypothesis was that the increase in the number of the aggregates would have led to the increase in the COF. The choice of the eight surfaces with aggregates was done so as to cover the most of the range of the coverage area

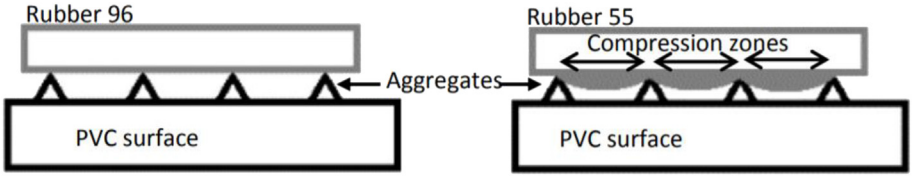

Fig. 3. The proposed hypothesis for the effect of the different hardness rubbers in measuring the friction coefficient at different contact levels for the same surface.

Table 1
The nine manufactured PVC – SiC aggregate composite surfaces with their planned coverage surface areas by the aggregates and the analytical plan for identification of the critical factor(s) affecting friction.

Sample number	0	1	2	3	4	5	6	7	8
Projected coverage area %	0	12.5	25	37.5	50	62.5	75	87.5	100

(0%100%), targeting both at the extreme values and also to detect, with the used controlled meshes, any correlation between the addition of the aggregates with the COF. In fact the upper limit close to 100% was chosen based on safety reasons from the provision used for the scattering and also on the visual inspection of the corresponding surfaces that appeared to be fully covered. The experimental investigation that followed is shown in Fig. 4.

The PVC plastisol was supplied by Vinnolit GmbH & Co. KG and had a viscosity of 42,000 cP. The SiC was supplied by Washington Mills and was according to the FEPA classification (Federation of European Producers of Abrasives) of size F30 or 600 μm. The plastisol was poured into square moulds with size 10 cm*10 cm with the attention not to include any air bubble that could introduce errors in the measurement of friction. Then the scattering of the aggregates took place randomly using a lab scale provision with a series of controlled meshes. The randomness refers to the position of the SiC aggregates on the surface that had no symmetry or pattern. Just after the aggregates addition, the samples were placed at an oven with the temperature of the curing to be 165°C for 90 s, in order to allow the full immobilization of the PVC chains that happens at 150°C as found from the literature [55]. Fig. 5 presents two representative surfaces developed for the present experimental investigation.

3. Results

3.1. Compositional analysis

Fig. 6 presents characteristic FTIR graphs for two PVC samples. FTIR analysis of all samples presented almost identical graphs with minute differences primarily with regards to the transmittance values, but with the peaks to have identical wavelength numbers. The main overarching structure of the PVC is –CH2-CH-Cl so the main wavenumbers expected were those from the alkane group. From 4000 cm^{-1} to 1500 cm^{-1} the general area of the graphs gave peaks at 2959 cm^{-1} and 2927 cm^{-1} that correspond to the C–H and C–H2 stretching modes, respectively, due to the presence of the main alkane structure of the PVC. However at 1718 cm^{-1} was detected a C=O stretching bond a fact that could be justified from the reaction of the PVC with the atmospheric oxygen whilst in the curing stage.

In the characteristic fingerprint region from 1500 cm^{-1} to 500 cm^{-1}, all the possible movements of the various structural units were detected from the FTIR spectrum. The absorption peaks of the individual groups were found for CH2 in phase bending (1425 cm^{-1}), CH out of phase bending (1334 cm^{-1}), CH rocking (1267 cm^{-1}; 1252 cm^{-1}) and C–Cl stretching (690 cm^{-1}). From 1102 cm^{-1} to 874 cm^{-1} the absorption bands correspond to the stretches of the main chains in parallel or perpendicularly to the plane of the chains [23]. The peak at 731 cm^{-1} was found to emanate from the rocking of the C–Cl bonds [56].

3.2. Calculation of the aggregates shape descriptors

The first variable under investigation was the minimum size of the aggregate as expressed by the minimum Feret dimension (see Table 2). In fact, the choice of the minimum Feret to assess the aggregates was justified from the separation of the aggregates at the stage of their production; only aggregates with maximum size equal to the minimum Feret number could pass from the openings of the F30 mesh. Aggregates that were bigger than the opening of the separation mesh during their production could still have passed from the mesh provided that their biggest dimension was equal or less than 600 μm. The measured minimum Feret number was shown to be in line with the values from the specifications and followed a normal distribution. The normal distribution was verified to be valid for the description of the aggregates according to Ref. [57].

Despite the a priori information for the size of the SiC aggregates from the supplier, their further analysis before their incorporation into the PVC was necessary, in order to quantify the rest of the geometrical variables (in addition to the average aggregate mean size). The reason for this analysis was to monitor that the inclusion of the aggregates into the PVC matrix, resulting into differences only in the spatial density of the aggregates and the %area of the aggregates.

In Fig. 7 the four techniques that were used for the measurement of the spatial densities of the aggregates are compared. The best method seemed to be the processing of the images with the ImageJ with no watershed. All the other techniques gave similar values up to 50 aggregates/cm^2 and then appeared to deviate for several reasons. Those reasons are explained below and varied depending on the mechanism of separation of the aggregates from the PVC.

More analytically, the use of ImageJ with watershed overestimated the spatial densities, on the one hand due to separation of aggregates that are not very close and on the other hand due to their shape that satisfied the mathematical conditions for watershed. More analytically the aggregates that are close enough appeared to produce a continuously bigger aggregate, after the thresholding, which was an artefact. In Fig. 7 that artefact was observed also in the microscopic calculation of the spatial densities, as it was unable to separate adjacent aggregates. The same overestimation is discussed also in other

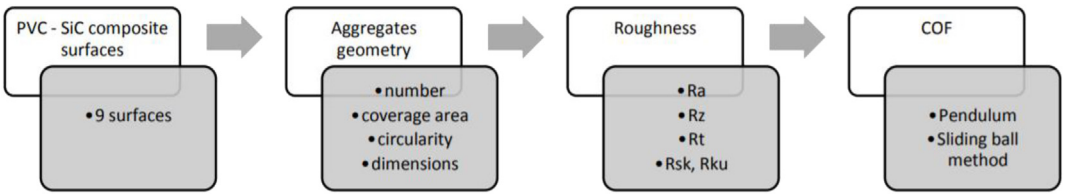

Fig. 4. Experimental investigation plan.

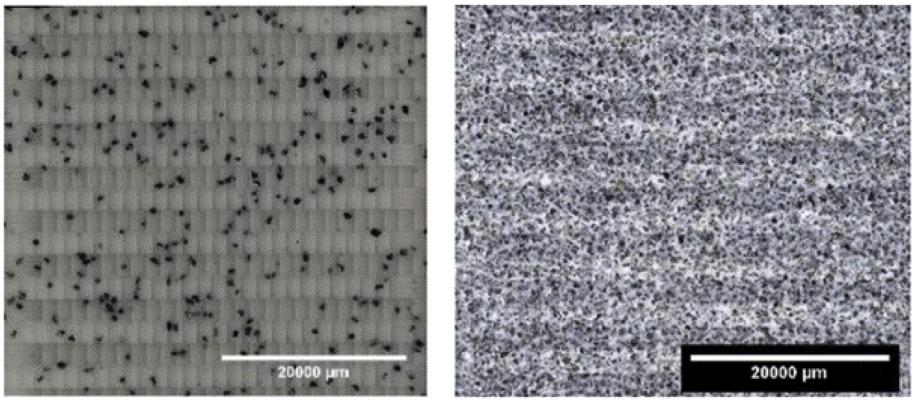

Fig. 5. Two representative PVC surfaces with the lowest (left) and the highest (right) surface percentages of SiC aggregates. The early correction of the surfaces high spatial aggregate densities, for a much brighter background from the acquisition from the microscope, was a necessity in order to use the ImageJ for a much clear delineation of the aggregates. The rectangle patterns emanate from the lighting effect of the microscope and had no effect in the image processing.

applications where the segmentation of digital images is necessary [58].

On the other hand the choice of the spatial densities from the gravimetric analysis seemed to make the final choice of the number of aggregates, according to the ImageJ method without watershed, more justifiable. The gravimetric analysis used the mean average size of the aggregates, as expressed by the average Feret number, and corrected for the circularity of the aggregates. The latter two variables were calculated from the ImageJ after the watershed was applied.

The circularity of the aggregates in all samples appeared to be consistent, *i.e.* 0.75 ± 0.11 - (see Table 2), and to follow the smallest extreme value distribution (EVD). That distribution appeared to justify better the presence of a small percent (long tail) of very elongated aggregates and a high frequency of more circular aggregates towards skewed towards the right. The smallest EVD was justified from the control of the minimum size of the aggregates on the circularity. The circularity was appeared not to be influenced by the watershed method providing evidence for similar mechanisms of incorporation of the aggregates during the curing of the PVC - composite surfaces.

Other studies have found that the effect of watershed can lead to erroneous description of the boundaries of the aggregates due to the difficulty of the image processing techniques to separate the shadowing effect from aggregates that are very close to each other [59]. However, the stability of the circularity for the surfaces with the low spatial densities of the aggregates, along with the same distributions describing the circularity supported further the argument of the similar mounting mechanisms of the aggregates on the PVC that led to a specific orientation of the aggregates. The stability of the aspect ratio (AR) and roundness (R) (see Table 2) added further support to the mounting mechanism of the aggregates.

The impact of circularity and spatial density of the aggregates is given in Fig. 8. In this figure, the theoretical % areas of the aggregates, as calculated from the gravimetric method, are compared with the real % areas as calculated from the ImageJ without the watershed. Those areas consist the vertical projections of each aggregate and not the real surfaces areas as would have calculated from a 3D topographic analysis. From Fig. 8, it is obvious that the maximum % area achieved was 37%, even for the surfaces with the greatest spatial density in aggregates. In the figure are presented the two extreme values of circularity according to the values of Table 2, with the more circular the aggregate was, the more surface area it occupied. The % areas as measured with the ImageJ without the application of the watershed algorithm were the same, despite the slightly greater number of aggregates than the theoretically calculated. The previous analysis of the increasing surface area with increasing circularity is validated from other studies on particle morphological studies [60].

Finally, with reference to the size of the aggregates, it can be shown in Table 2 a decrease in the size of the aggregates when more aggregates are added (see Fig. 9). In Fig. 9 the addition of more aggregates (up to 180 aggregates/cm^2 or equivalently 24%wt.) seemed to have led to a twofold or threefold reduction of the size of the aggregates. This was expected due to the segmentation of the aggregates from the watershed method. That cause had a small impact on the size from close inspection of the images before analysed and after the application of the watershed algorithm. On the other hand, the increase in weight per area of the aggregates was attributed to cause a decrease in the size of the aggregates due to increased displacement of the PVC paste before curing. That displacement seemed to have caused greater immersion of the aggregates, a fact that was further supported by the literature [61].

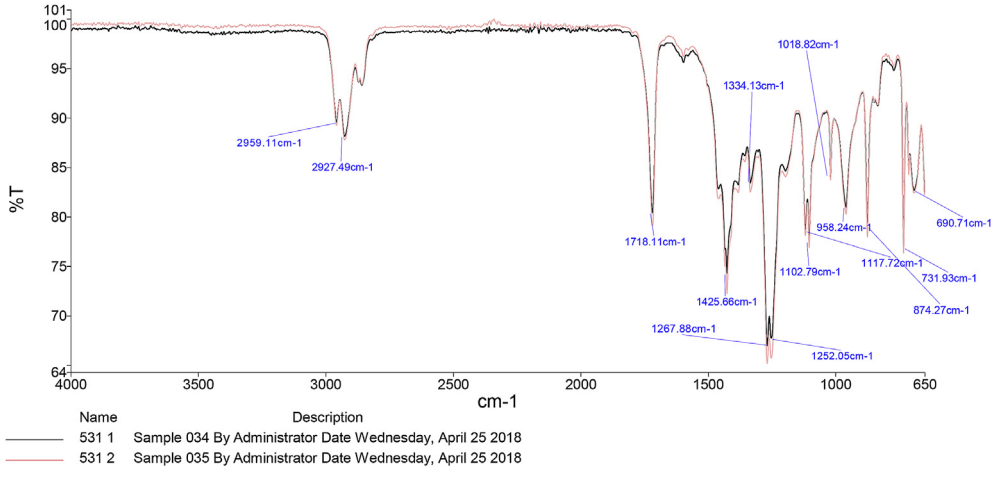

Fig. 6. FTIR graphs for two characteristic PVC samples.

Table 2
The calculated geometrical parameters of the aggregates in the PVC - aggregate composite surfaces, as calculated with the ImageJ using the watershed method. 3. Note: the %Area corresponds to the projected area of the aggregates in the horizontal plane of the main PVC matrix and not the area of the exposed volume of the aggregate.

	a_i /cm^2	%Area	*C*	*R*	Solidity	*AR*	Major	Minor	Feret	
									Min.	$\bar{x}$
Raw ag.		–	0.77 ± 0.07	0.78 ± 0.12	0.94 ± 0.03	1.31 ± 0.23	812 ± 136	566 ± 112	587 ± 110	859 ± 124
1	19 ± 3	4 ± 1	0.75 ± 0.12	0.71 ± 0.15	0.87 ± 0.08	1.48 ± 0.37	666 ± 136	408 ± 137	442 ± 154	707 ± 218
2	27 ± 2	8 ± 1	0.71 ± 0.15	0.70 ± 0.16	0.91 ± 0.06	1.47 ± 0.34	731 ± 315	455 ± 155	521 ± 232	751 ± 191
3	49 ± 6	13 ± 2	0.73 ± 0.16	0.70 ± 0.16	0.91 ± 0.06	1.54 ± 0.44	624 ± 187	432 ± 139	454 ± 143	688 ± 160
4	214 ± 10	31 ± 1	0.71 ± 0.09	0.69 ± 0.15	0.93 ± 0.03	1.37 ± 0.27	458 ± 272	314 ± 198	335 ± 211	496 ± 296
5	202 ± 15	27 ± 1	0.73 ± 0.09	0.68 ± 0.15	0.93 ± 0.03	1.38 ± 0.28	297 ± 215	199 ± 149	213 ± 160	322 ± 233
6	332 ± 30	34 ± 5	0.72 ± 0.11	0.68 ± 0.15	0.89 ± 0.06	1.38 ± 0.28	251 ± 183	168 ± 125	180 ± 135	273 ± 199
7	225 ± 5	37 ± 3	0.79 ± 0.10	0.76 ± 0.13	0.93 ± 0.03	1.37 ± 0.27	374 ± 228	250 ± 154	268 ± 167	405 ± 248
8	235 ± 3	35 ± 1	0.74 ± 0.11	0.69 ± 0.15	0.93 ± 0.04	1.37 ± 0.28	330 ± 220	220 ± 148	236 ± 160	357 ± 238

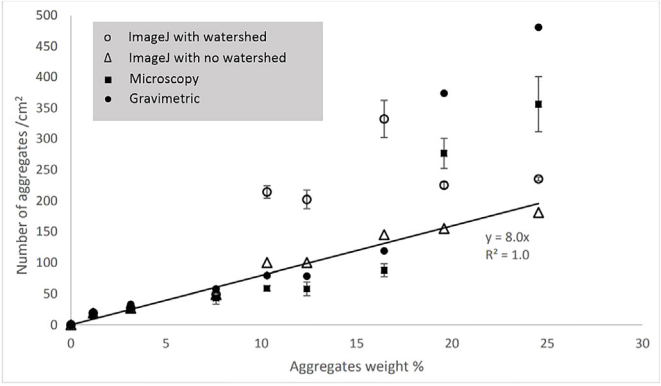

Fig. 7. Comparison of the three techniques (gravimetric, microscopic, ImageJ with and without watershed) for measuring the aggregates spatial density; The triangle represents the number of aggregates measured with ImageJ with no watershed to spate it from the ImageJ processing with watershed.

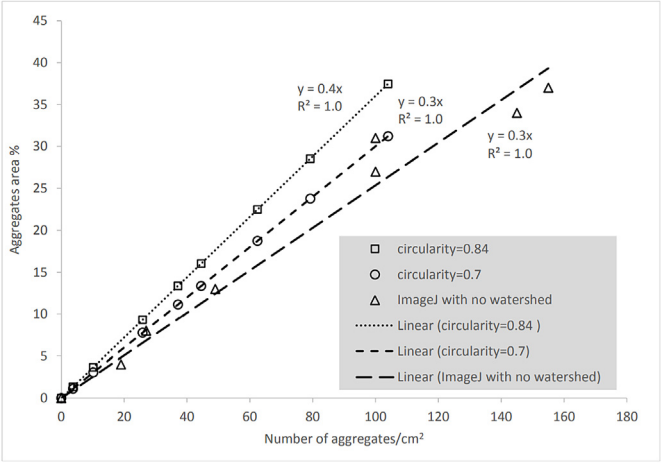

Fig. 8. Comparison of the two techniques (gravimetric, ImageJ without watershed) for measuring the aggregates coverage area.

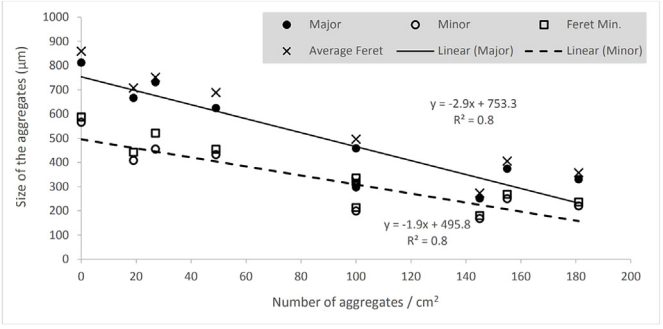

Fig. 9. The sizes of aggregates in the various PVC – aggregate composite surfaces in different measuring directions.

3.3. Roughness analysis

Fig. 10 shows the impact of the number of aggregates on the examined roughness parameters. The impact of the increasing spatial densities of aggregates seemed to have no impact on the skewness and kurtosis of the roughness profiles (see Fig. 10C and D). The positive Rsk suggested that the domination of peaks in the roughness profile emanating from the SiC aggregates. The similar values of Rsk in all samples suggested that the addition of aggregates did not seem to change the distribution of the peaks. The shape of those peaks was given by the Rku values (greater than 3) that suggested the domination of sharp peaks with less round shape. The values of the roundness presented in Table 1 justify the shape of the peaks according to the Rku. Previous research on the shape of the aggregates has shown that values of roundness around 0.7 would have given Rku less than 3 with less sharp peaks [62]. However, close inspection of the distribution of the roundness at the embedded aggregates in the PVC matrix revealed angular particles from 0.4 to 0.5 that justifies the sharpness of the peaks.

On the other hand, the increased number of aggregates and the % coverage area of the aggregates seemed to correlate well with the Ra and Rt with less correlations with the Rz (see Fig. 10A and B). The values of the overall roughness as expressed by Ra appeared to have values up to 23 µm, the Rz up to 150 µm and the Rt up to 250 µm. For the nine surfaces examined in this paper the Ra and Rz values seemed to correlate to each other. The main reason for this was the smoothness of

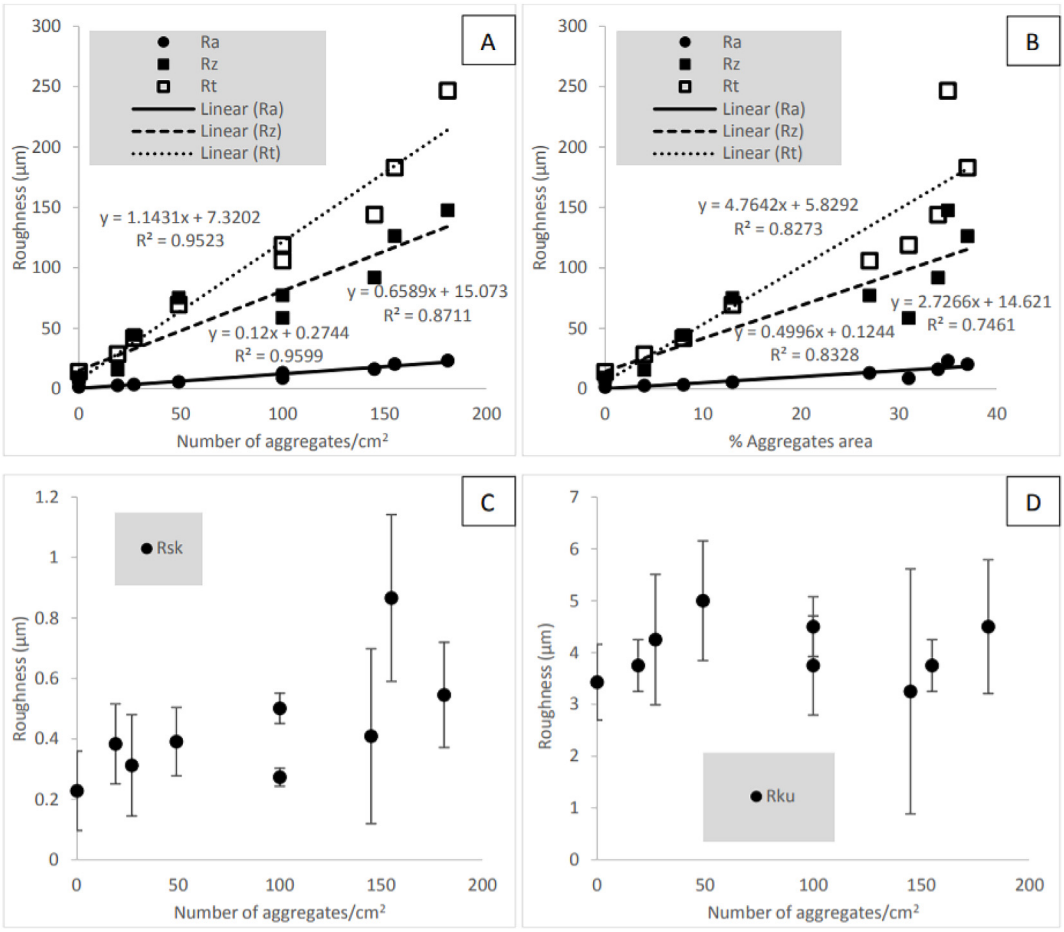

Fig. 10. The correlation of the Ra, Rz and Rt with the spatial densities (A) and coverage areas (B) of the aggregates; the correlation of the (C) Rsk and (D) Rku with the number of aggregates.

the surface created by the PVC matrix and the fact that the roughness was controlled mainly by the peaks of the deposited SiC aggregates.

More analytically, the attachment of the aggregates to the PVC appeared not to have any distinct valleys from close inspection of their interfaces; fact that was reflected at the Rku values. Thus, the main mechanism of altering the roughness Ra was the addition of more aggregates that increased the centre line average (CLA) up to 23 µm (see Fig. 10A). The CLA appeared to increase mainly due to the increase of the main line of definition of the CLA towards the peaks of the aggregates, *i.e.* the equation of the surface areas below and above a horizontal line across the roughness profile [63]. A much more rigorous analysis of Ra, Rz and Rt from Fig. 10A demonstrated their linear correlation, and thus their indiscriminate usage for the particular PVC-aggregate composite surfaces (see Fig. 11).

3.4. Coefficient of friction

The COF was measured with the techniques of british pendulum in wet conditions and scratch testing in dry conditions for the nine PVC-aggregate composite surfaces. The pendulum test values (PTV) were measured per surface. Thus based on the PTV and the equation presented by Ref. [46], the COF was calculated. The PTV was measured only in surfaces that were covered with water since the dry measurements would have resulted to severe degradation of the rubber of the slider and thus erroneous results towards the more dense surfaces. The degradation, on the one hand meant more sliders to be used and one the other hand, more importantly, big differences in the measurements even for the same surface.

The results of the COF from the PTV values are presented in Fig. 12

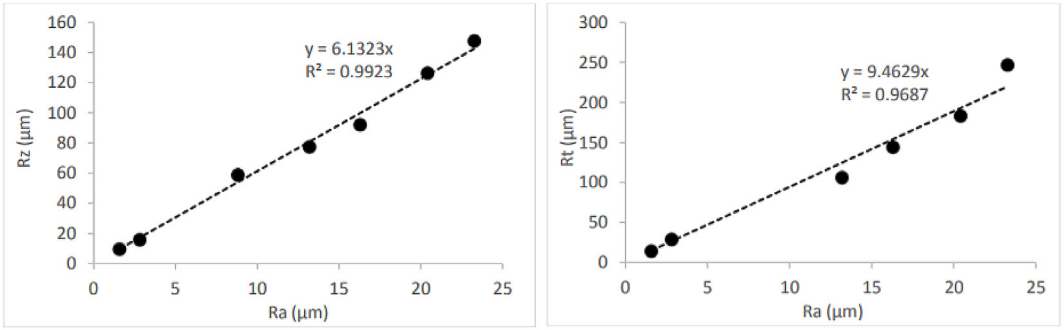

Fig. 11. The correlation between the roughness parameters Ra, Rz and Rt.

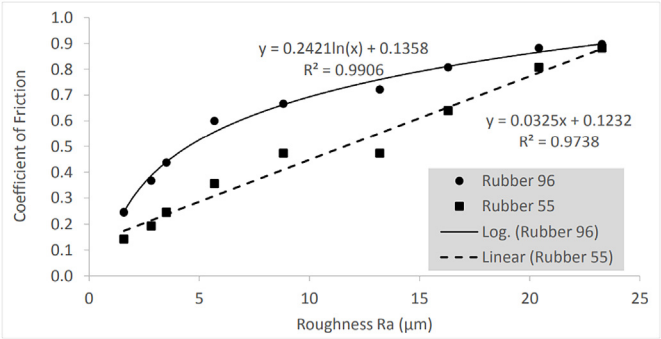

Fig. 12. The relationship between the COF, as calculated from the PTV for the two rubbers used, with Ra.

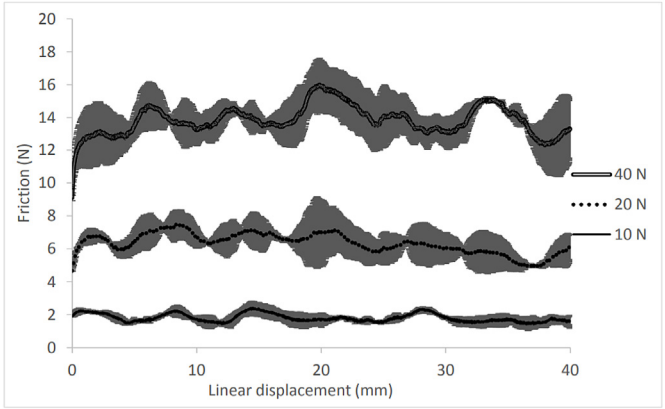

Fig. 13. The friction force measurement versus the linear displacement during the dry sliding of the chrome steel ball on the pure PVC surfaces with no aggregates; for all the other surfaces the same procedure was implemented.

as a function of the Ra. The COF was shown to depend not only on roughness but also on the type of rubber. The COF, for the hardest rubber 96, appeared to be a function of the logarithm of Ra, while the COF for the softest, 55, appeared to follow a linear trend with Ra.

The dependence of the COF on the type of rubber is a documented fact [64]. Thus the observed increased values of COF using the hardest rubber, for each surface, in comparison to the rubber 55 are well justifiable (see Fig. 12). It is evident that the hardest the rubber, therefore the less compressible will be the rubber and thus the contact points between the rubber and the examined surface will be mostly the peaks of the aggregates. In addition, due to the increase in the number of the spatial density of the aggregates, the contact asperities with the rubber will be limited to the aggregate peaks and not to the entire PVC-aggregate surface area.

That contact of the rubber with the top of the aggregates was found in the literature to be a well-established phenomenon in the friction of a harder with an softer solid [65]. That phenomenon gave rise to the non-linear correlation between the COF and Ra in the present study. That non-linear correlation was justified on the basis of the interaction of the harder rubber (see Fig. 12), with the representation of the counter surface with the roughness to be represented by a power spectrum correlation [48]. That power spectrum correlation for polymers was found to be logarithmic when the friction and normal forces are expressed in the form of shear stress and shear rate, owning to the equilibrium barrier that is formed in the case of prolonged static contact of two polymers [66].

The logarithmic relationship between the COF from pendulum testing and Ra was documented from the literature [67]. In other words expressing the logarithmic trend-line (Fig. 12) as exponential $R_a = e^{(COF-0.14)/0.24}$.

Due to the representation of the power spectrum of the surface topography by Ra and the equilibrium energy barrier for sliding, due to the asperities interlocking due to static conditions, by the COF then the exponential form of Ra with COF is an Arrhenius type equation well known to describe the friction of polymer-like surfaces [68]. On the other hand, the linear correlation between the rubber 55 COF and Ra appeared to be in line with the Coulomb–Amonton's law [69], *i.e.* the COF increased linearly by increasing the roughness Ra, with no other obvious dependence of the COF on the surface area of the aggregates but only on the number of them.

With reference to the calculation of the COF from the scratch test under constant load and dry conditions, Fig. 13 summarizes the procedure for the measurement of the friction forces. From Fig. 13, it appeared that the friction forces depend on the normal load and that by increasing the normal forces the associated heterogeneities of the PVC were magnified. Fig. 13 gives exactly the same procedure that was used to calculate the mean friction force for each PVC-aggregate composite surface. The relation between the mean friction forces in dry conditions and the normal forces is given in Fig. 14-A, and appeared to be linear with the gradient to be equal to the COF. Despite the phenomenological overlapping of the data, there were observed clear differences of the COF for each PVC-aggregates as given in Table 3. It is notable the fact that while those COF range from 0.38 to 0.45, the COF from the pendulum ranged from 0.25 to 0.81 for rubber 96 and from 0.14 to 0.64 for rubber 55.

Fig. 14-B gives the relationship between the COF calculated with the scratch testing device in dry conditions and the british pendulum in wet conditions. A first observation is the very good linear fitting between two independent techniques. After extrapolation of the trendlines for very low COF from the pendulum, the corresponding COF from the scratch testing is found to be 0.34 and 0.36 for rubbers 96 and 55 respectively. These values from pendulum can be assigned to the inherent friction due to the mechanical friction that occurs even in lubricated conditions that give rise to the effective friction [70]. In other words the two surfaces, even covered with a liquid film, still have an inherent friction due to the asperities; that friction however is depressed from the low spatial density of the aggregates that are unable to inhibit the losses of friction towards lower COFs than that calculated from the scratch testing provision.

Additionally, Fig. 14-B shows the overestimation of the COF from the British pendulum for values greater than 0.4 and the underestimation of the COF for x values less than 0.4. That phenomenon was explained from the lack of 1-1 correspondence of the values of the COF and can be justified from the mechanisms of measurement of the two methods. On the one hand, the pendulum under wet conditions provides the COF during: (1) sliding of the rubber on a hydrodynamic water film and (2) plastic deformation of the slider. On the other hand the scratch testing measures the mechanical friction with no wear of the measuring medium of friction force. In other words, the small spatial densities of the aggregates seemed to enhance the hydrodynamic lubrication upon rubber sliding, fact that suggests the underestimation of the COF. While at low spatial densities, it would have been anticipated COF greater than 0.38 according to the scratch testing, in fact the impact of surface chemistry seemed to have decreased the mechanical COF by enhancing the lubrication.

On the other hand, the overestimation of the COF from the pendulum in comparison to the scratch testing suggested either: (1) a possible impact of the wear of the slider in the course of the measurement, or (2) more effective pathways of removal of the wet film due to the increased roughness of the surface. Fig. 14-B shows that the reported values of the COF using the harder slider are higher than those of the softer for the same mechanical COF. That fact reinforces the hypothesis of Fig. 3, according to which the hardest rubber develops friction with the peaks of the aggregates and less with the main PVC matrix. In the case of the softest rubber, its penetration into the space among the aggregates seemed to have created compression zones that

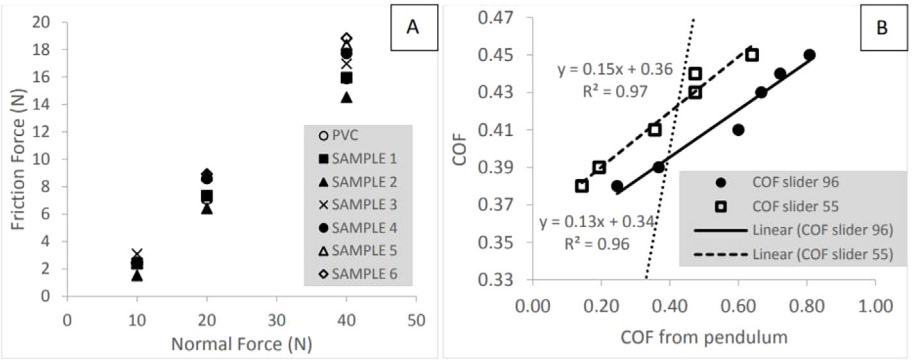

Fig. 14. The calculation of the COF for each surface from the graph of friction versus normal forces (A); the comparison of the COF as calculated from the scratch test under constant load and the british pendulum (the dotted line is the (0,0)-(1,1) line).

Table 3
The calculated COF from Fig. 14-A as the gradient of the friction-to-normal forces for each PVC and PVC-aggregate composite surface.

	PVC (0)	1	2	3	4	5	6
COF	0.38	0.39	0.40	0.41	0.43	0.44	0.45

have slid onto the water film and reduced the overall COF. The surfaces in all cases appeared will less friction in the case of the softer rubber, highly possibly due to the lack of effective removal of the squeeze film owning to the inherent wetness of the surface that was also observed elsewhere [71]. Hence the mechanical friction must be taken into consideration in order to understand the impact of the adhesive friction [72] in materials that are mechanically instable due to viscoelasticity [73].

No bias in the values of COF can be assigned to the measurement of the COF using a soft (rubber) and a hard (steel) counterface. As seen in Fig. 14-B the measurement of the COF from the pendulum seems to cause the lack of 1-1 matching when water is present. In other words, the design of the produced PVC-aggregate composite surfaces, appear to have a wide range of COF (0.16–0.80) that corresponds to a small range of friction (0.37–0.45) when measured with the scratching method.

During the friction coefficient measurement with the stylus method, the steel ball experiences micro-scratches during the measurement across a surface due to the aggregates. However, the replacement of the steel ball with a new for each surface, certifies that the friction measurement is done with no effects of a used steel ball to the next surface. The impact of high loads up to 40 N seemed to have had no impact for both steel ball and measured surface.

The lack of adhesion of the rubber sliders with the PVC matric was evident. If adhesion was significant then at low spatial densities of the aggregates, the COF from the pendulum testing would have been close to the line segment (0,0),(1,1). However, since the rubbers slider reach the surface at a certain speed, with the presence of water and they were not in contact for a long time allowing enough van der Waals forces to be developed, adhesion was assigned to be negligent in comparison to the friction force due to asperities contact as found previously [74].

The use of the scratch testing for measurement the COF in the examined surfaces has never been attempted before, to the best of the knowledge of the authors. Despite the phenomenological different mechanisms of measurement, in fact the two techniques provide complementary information for the friction mechanism verifying previous research [75]. First of all, there was proved to be a linear relation between methods that measure COF in terms of a single asperity (stylus) and multiple asperities (slider). This scaling-up problem from single to multiple asperities has been identified as the key for understanding the friction mechanism [76,77]. Secondly, it was shown that below COF = 0.4 the multiple asperities are unable to provide additional energy to provide mechanical friction with values similar to the single asperity and thus the values of COF reach very low values (COF = 0.16). Above COF = 0.4, it seemed that the presence of multiple asperities inhibit effectively the liquid film formation and provide a surplus of frictional energy above the requirements for friction at a single asperity. That observation agrees with previous research for the dependence of the friction coefficient on the size of the friction measuring device [78]. Also the existence of a threshold above witch adhesion does not enhance friction, but the roughness and asperities govern friction [79], is highly promising in commercially available surfaces with controlled COF from their nanostructure [54].

The two methods for measuring the friction coefficient, despite their differences in the contact surface area, in fact represent the similar effects of the number of aggregates on the friction. Whether friction is measured from a stylus (point analysis) or a slider (surface analysis), it is presumed that the positioning of the aggregates, from their random scattering, to have similar effect on the friction coefficient measurement despite the surface area. In other words, the sliding of the stylus was assumed to depend on the number of the aggregates the same way that the rubber slider depended upon during sliding. The previous statement in fact assumes that the scattering of the aggregates is isotropic both in the direction of the stylus movement, as in the perpendicular direction of the sliding of the rubber slider. Whereas the slider measures the COF of multiple aggregates simultaneously, the stylus method measures the friction coefficient across a line of those aggregates, but based on their increased spatial density over the measurement line.

The calculated friction coefficient from the pendulum testing was found to depend on the hardness of the counterface of the slider. In fact, the friction coefficient between two rubber materials depends on multiple factors like surface chemistry, surface finish, time of contact and speed of sliding that makes imperative the use of a method, which keeps the properties of the measuring material almost unchanged. Thus the use of a stylus method has provided the friction coefficient due to the mechanical barriers of the interlocking of the stylus ball with the aggregates. The constant friction coefficient for a constant normal load proved that each aggregate had a similar interlocking mechanism despite its random orientation. Complementary to that, the friction coefficient as calculated from the frictional-normal load graph provides a different perspective of the coefficient, than that calculated from the pendulum. In fact the friction coefficient from the stylus measurements, can act as a baseline for comparing the different counterfaces *i.e.* whether the lubrication lowers the stylus measured friction or the adhesive or ploughing effects increase the stylus measured friction.

4. Conclusions

In the present paper, the tribological characteristics of PVC surfaces when dispersing SiC aggregates were investigated. Both the measuring

methods adopted and tested, as well the findings of the measurements were discussed. For such surfaces, the optimum 2D imaging analysis method for the calculation of the geometry of the aggregates on the PVC-aggregate composite surfaces was proposed. According to the authors' knowledge this is the first time that such a study has been presented. PVC − SiC aggregate composite surfaces were manufactured up to 235 aggregates per cm^2 and 35% surface coverage area.

The main findings of the experimental investigation are:

1. The incorporation mechanism of the SiC aggregates on the surfaces appeared to be the same. That mechanism consisted of the surface exposure of the sharpest edges of the aggregates as evidenced from the roughness Rsk and Rku.
2. The analysis of the COF for the PVC-aggregates composite surfaces demonstrated the dependence of the COF on the counterface. For the first time, two experimental techniques for measurement of COF in a particular case of tribological surfaces, the one based on single asperity measurements (steel ball stylus) and the other on multiple asperity (pendulum), were found to have a linear correlation.
3. The mechanism of friction for a rubber as counterface was explained from the presence of the hydrodynamic liquid film and the multiple asperities (mechanical part of friction) appeared unable to prevent the friction losses below 27 ± 2 SiC aggregates/cm^2.
4. The translation of the COF, that is measured with a rubber counterface, to the COF, as measured with a non-degraded counterface, has demonstrated a small range of true mechanical –overall- friction that was found to be easily lost due to the presence of a liquid film.

Such findings suggest the importance of a further study of the surface chemistry on the design of PVC composite surfaces with the desired COF.

Acknowledgements

The research was partially funded by the Engineering and Physics Research Science Council UK (Grant Number EP/L016389/1). Data underlying this study can be accessed through the Cranfield University repository at https://doi.org/10.17862/cranfield.rd.9742739.

Appendix A. Supplementary data

Supplementary data to this article can be found online at https://doi.org/10.1016/j.triboint.2019.105906.

References

[1] Bhaduri D, Batal A, Dimov SS, Zhang Z, Dong H, Fallqvist M, et al. On design and tribological behaviour of laser textured surfaces. Procedia CIRP 2017;60:20–5. https://doi.org/10.1016/J.PROCIR.2017.02.050.
[2] Lu P, Wood RJK, Gee MG, Wang L, Pfleging W. A novel surface texture shape for directional friction control. Tribol Lett 2018;66:51. https://doi.org/10.1007/s11249-018-0995-0.
[3] Chen P, Li X, Ma J, Zhang R, Qin F, Wang J, et al. Bioinspired photodetachable dry self-cleaning surface. Langmuir 2019;35:6379–86. https://doi.org/10.1021/acs.langmuir.8b04310.
[4] Spurr RT. The friction of polymers. Wear 1982;79:301–10. https://doi.org/10.1016/0043-1648(82)90320-9.
[5] Clark AJ, Higham TE. Slipping, sliding and stability: locomotor strategies for overcoming low-friction surfaces. J Exp Biol 2011;214. https://doi.org/10.1242/jeb.051136. 1369 LP-1378.
[6] Bell JL, Collins JW, Wolf L, Grönqvist R, Chiou S, Chang W-R, et al. Evaluation of a comprehensive slip, trip and fall prevention programme for hospital employees. Ergonomics 2008;51:1906–25. https://doi.org/10.1080/00140130802248092.
[7] Miller JM. "Slippery" work surfaces: towards a performance definition and quantitative coefficient of friction criteria. J Saf Res 1983;14:145–58. https://doi.org/10.1016/0022-4375(83)90042-7.
[8] Sannareddy H, Raja J, Chen K. Characterization of surface texture generate multi-process manufacture. Int J Mach Tool Manuf 1998;38:529–36. https://doi.org/10.1016/S0890-6955(97)00098-9.
[9] Stead IMN, Eckold DG, Clarke H, Fennell D, Tsolakis A, Dearn KD. Towards a plastic engine: low—temperature tribology of polymers in reciprocating sliding. Wear 2019;430–431:25–36. https://doi.org/10.1016/J.WEAR.2019.04.008.
[10] Lan P, Zhang Y, Dai W, Polycarpou AA. A phenomenological elevated temperature friction model for viscoelastic polymer coatings based on nanoindentation. Tribol Int 2018;119:299–307. https://doi.org/10.1016/J.TRIBOINT.2017.11.009.
[11] Vakis AI, Yastrebov VA, Scheibert J, Nicola L, Dini D, Minfray C, et al. Modeling and simulation in tribology across scales: an overview. Tribol Int 2018;125:169–99. https://doi.org/10.1016/J.TRIBOINT.2018.02.005.
[12] Pitenis A, Manuel Urueña J, Mcghee E, Hart S M, Reale E, Kim J, et al. Challenges and opportunities in soft tribology. Tribol Mater Surf Interfaces 2017;11(4):180–6. https://doi.org/10.1080/17515831.2017.1400779.
[13] Myshkin NK, Petrokovets MI, Kovalev AV. Tribology of polymers: adhesion, friction, wear, and mass-transfer. Tribol Int 2005;38:910–21. https://doi.org/10.1016/J.TRIBOINT.2005.07.016.
[14] Chandrasekar V, Janes DW, Forrey C, Saylor DM, Bajaj A, Duncan TV, et al. Improving risk assessment of color additives in medical device polymers. J Biomed Mater Res B Appl Biomater 2018;106:310–9. https://doi.org/10.1002/jbm.b.33845.
[15] Salmeia KA, Gooneie A, Simonetti P, Nazir R, Kaiser J-P, Rippl A, et al. Comprehensive study on flame retardant polyesters from phosphorus additives. Polym Degrad Stab 2018;155:22–34. https://doi.org/10.1016/J.POLYMDEGRADSTAB.2018.07.006.
[16] Hahladakis JN, Velis CA, Weber R, Iacovidou E, Purnell P. An overview of chemical additives present in plastics: migration, release, fate and environmental impact during their use, disposal and recycling. J Hazard Mater 2018;344:179–99. https://doi.org/10.1016/J.JHAZMAT.2017.10.014.
[17] Bogoeva-Gaceva G, Dimeski D, Srebrenkoska V. Friction mechanism of polymers and their composites. Macedonian J Chem Chem Eng 2018;37(1):1–11. https://doi.org/10.20450/mjcce.2017.1407.
[18] Hisakado T, Suda H, Watanabe H. The friction and wear mechanisms between ceramics and metals. Wear 1992;155:251–68. https://doi.org/10.1016/0043-1648(92)90085-M.
[19] Pei X-Q, Lin L, Schlarb A, Bennewitz R. Contact area and shear stress in repeated single-asperity sliding of steel on polymer. Tribol Lett 2019;67:30. https://doi.org/10.1007/s11249-019-1146-y.
[20] Jiang C, Jiang H, Zhang J, Kang G. Analytical model of friction behavior during polymer scratching with conical tip. Friction 2018. https://doi.org/10.1007/s40544-018-0225-7.
[21] Weber B, Suhina T, Junge T, Pastewka L, Brouwer AM, Bonn D. Molecular probes reveal deviations from Amontons' law in multi-asperity frictional contacts. Nat Commun 2018;9:888. https://doi.org/10.1038/s41467-018-02981-y.
[22] Mikhin NM, Lyapin KS. Hardness dependence of the coefficient of friction. Sov Phys J 1970;13:317–21. https://doi.org/10.1007/BF00818317.
[23] Bahadur S, Tabor D. The wear of filled polytetrafluoroethylene. Wear 1984;98:1–13. https://doi.org/10.1016/0043-1648(84)90213-8.
[24] Bailey EWM. The effect of embossing process conditions on the surface properties of a plasticized vinyl polymer. University of Massachusetts Amherst; 1984.
[25] Ferry JD, Landel RF. Molecular friction coefficients in polymers and their temperature dependence. Kolloid Z 1956;148:1–6. https://doi.org/10.1007/BF01501955.
[26] Berardo A, Costagliola G, Ghio S, Boscardin M, Bosia F, Pugno NM. An experimental-numerical study of the adhesive static and dynamic friction of micro-patterned soft polymer surfaces. Mater Des 2019;181:107930. https://doi.org/10.1016/J.MATDES.2019.107930.
[27] Voyer J, Klien S, Velkavrh I, Ausserer F, Diem A. Static and dynamic friction of pure and friction-modified PA6 polymers in contact with steel surfaces: influence of surface roughness and environmental conditions. Lubricants 2019;7. https://doi.org/10.3390/lubricants7020017.
[28] Shen M, Zhang Z, Yang J, Xiong G. Wetting behavior and tribological properties of polymer brushes on laser-textured surface. Polymers 2019;11. https://doi.org/10.3390/polym11060981.
[29] Magnoni M, Giustozzi F. Evaluation of the effect of aggregates mineralogy and geometry on asphalt mixture friction. J Civ Environ Eng 2016;6:223. https://doi.org/10.4172/2165-784X.1000223.
[30] Persson B, Tartaglino U, Albohr O, Tosatti E. Rubber friction on wet and dry road surfaces: the sealing effect. Phys Rev B 2015;71:035428https://doi.org/10.1103/PhysRevB.71.035428.
[31] Mutlu İ, Sugözü İ, Keskin A, Mutlu İ, Sugözü İ, Keskin A. The effects of porosity in friction performance of brake pad using waste tire dust. Polímeros 2015;25:440–6. https://doi.org/10.1590/0104-1428.1860.
[32] Pawlak Z, Urbaniak W, Kałdoński T, Oloyede A. Importance of bearing porosity in engineering and natural lubrication. Biomater Med Tribol Res Dev 2013:44. https://doi.org/10.1533/9780857092205.311.
[33] Briscoe BJ, Tabor D. Friction and adhesion. Surface forces in friction and adhesion. Faraday Spec Discuss Chem Soc 1972;2:7–17. https://doi.org/10.1039/S19720200007.
[34] Maeda N, Chen N, Tirrell M, Israelachvili JN. Adhesion and friction mechanisms of polymer-on-polymer surfaces. Science 2002;297. https://doi.org/10.1126/science.1072378. 379 LP-382.
[35] Vaziri M, Stott FH, Spurr RT. Studies of the friction of polymeric materials. Wear 1988;122:313–27. https://doi.org/10.1016/0043-1648(88)90017-8.
[36] Gauthier C, Lafaye S, Schirrer R. Elastic recovery of a scratch in a polymeric surface: experiments and analysis. Tribol Int 2001;34:469–79. https://doi.org/10.1016/S0301-679X(01)00043-3.
[37] Mostafavi S, Tong F, Dugger T, Kisailus D, J Bardeen C. Non-covalent photochromic polymer adhesion. Macromolecules 2018;51(6):2388–94. https://doi.org/10.1021/acs.macromol.8b00036.

[38] Salehani K. Modelling adhesion and friction in contact problems. Delft University of Technology; 2019. https://doi.org/10.4233/uuid:d53f2842-480c-4cf2-b8c7-cbaf157d4398.
[39] Tiwari A. Adhesion, friction and leakage in contacts with elastomers. Norwegian University of Science and Technology; 2018.
[40] Myshkin NK, Kovalev AV. Adhesion and friction OF polymers. Polym. Tribol. IMPERIAL COLLEGE PRESS; 2009. p. 3–37. https://doi.org/10.1142/9781848162044_0001.
[41] Sahli R, Pallares G, Ducottet C, Ben Ali IE, Al Akhrass S, Guibert M, et al. Evolution of real contact area under shear and the value of static friction of soft materials. Proc Natl Acad Sci 2018;115. https://doi.org/10.1073/pnas.1706434115. 471 LP-476.
[42] Fürstner R, Barthlott W, Neinhuis C, Walzel P. Wetting and self-cleaning properties of artificial superhydrophobic surfaces. Langmuir 2005;21(3):956–61. https://doi.org/10.1021/la0401011.
[43] Marmur A. The role of thin films in wetting. Rev Phys Appl 1988;23:1039–45.
[44] Stromberg RR, Straus S, Achhammer BG. Infrared spectra of thermally degraded poly(vinyl-chloride). J Res Natl Bur Stand 1958;60(2):147. https://doi.org/10.6028/jres.060.018.
[45] Chang W-R, Hirvonen M, Grönqvist R. The effects of cut-off length on surface roughness parameters and their correlation with transition friction. Hum Factors Ergon Soc Ann Meet Proc 2004;42(8):755–69. https://doi.org/10.1016/j.ssci.2004.01.002.
[46] Clarke J, Hallas K, Lewis R, Thorpe S, Hunwin G, Carré M. Understanding the friction measured by standardised test methodologies used to assess shoe-surface slip risk. J Test Eval 2015;43:4. https://doi.org/10.1520/JTE20120334.
[47] ASTM. Standard test method for measuring surface frictional properties using the British pendulum tester vol. 6. 1993.
[48] Persson BNJ, Albohr O, Tartaglino U, Volokitin AI, Tosatti E. On the nature of surface roughness with application to contact mechanics, sealing, rubber friction and adhesion. J Phys Condens Matter 2005;17:R1–62. https://doi.org/10.1088/0953-8984/17/1/R01.
[49] Yashima S, Takase N, Kurokawa T, Ping Gong J. Friction of hydrogels with controlled surface roughness on solid flat substrates. Soft Matter 2014;10:3192–9. https://doi.org/10.1039/c3sm52883a.
[50] Salt GF. (U.S.). NRC, Board. TR. Conference ISP. Research on skid-resistance at the transport and road research laboratory (1927-1977). Crowthrone, eng. Transport and Road Research Laboratory; 1977.
[51] Kosgolla JV. Numerical simulation of sliding friction and wet traction force on a smooth tire sliding on a random rough pavement. University of South Florida; 2012.
[52] Fuentes L. Investigation of the factors influencing skid resistance and the international friction index. 2019.
[53] Brzezinka TL, Rao J, Chowdhury M, Kohlscheen J, Fox Rabinovich GS, Veldhuis SC, et al. Hybrid Ti-MoS2 coatings for dry machining of aluminium alloys. Coatings 2017;7. https://doi.org/10.3390/coatings7090149.
[54] Tang J, Ding Q, Zhang S, Wu G, Hu L. Improved tribological performance of amorphous carbon (a-C) coating by ZrO_2 nanoparticles. Mater (Basel, Switzerland) 2016;9:795. https://doi.org/10.3390/ma9100795.
[55] López J, Balart R, Jiménez A. Influence of crystallinity in the curing mechanism of PVC plastisols. J Appl Polym Sci 2004;91:538–44. https://doi.org/10.1002/app.13122.
[56] Litvinov VM, De PP. Spectroscopy of rubbers and rubbery materials. Rapra Technology; 2002.
[57] Gu X, Tran Y, Hong L. Quantification of coarse aggregate shape in concrete. Front Struct Civ Eng 2014;8:308–21. https://doi.org/10.1007/s11709-014-0266-6.
[58] Wang W, Paliwal J. Separation and identification of touching kernels and dockage components in digital images. Can Biosyst Eng 2006;48:7.1–7.
[59] Butler JB, Lane SN, Chandler JH. Automated extraction of grain-size data from gravel surfaces using digital image processing. J Hydraul Res 2001;39:519–29. https://doi.org/10.1080/00221686.2001.9628276.
[60] Moosakazemi F, Tavakoli Mohammadi MR, Mohseni M, Karamoozian M, Zakeri M. Effect of design and operational parameters on particle morphology in ball mills. Int J Miner Process 2017;165:41–9. https://doi.org/10.1016/J.MINPRO.2017.06.001.
[61] Haywood A. The effect of polymer solutions on the settling behaviour of sand particles. The University of Manchester; 2011.
[62] Janoo V. Quantification of shape, angularity, and surface texture of base course materials 1998. Report 98-1 https://rosap.ntl.bts.gov/view/dot/14065.
[63] Nowicki B. Multiparameter representation of surface roughness. Wear 1985;102:161–76. https://doi.org/10.1016/0043-1648(85)90216-9.
[64] Kalacska G. An engineering approach to dry friction behaviour of numerous engineering plastics with respect to the mechanical properties. Express Polym Lett 2013;7(2):199–210. https://doi.org/10.3144/expresspolymlett.2013.18.
[65] Mahboob Kanafi M, Tuononen AJ. Top topography surface roughness power spectrum for pavement friction evaluation. Tribol Int 2017;107:240–9. https://doi.org/10.1016/J.TRIBOINT.2016.11.038.
[66] Müser MH, Urbakh M, Robbins MO. Statistical mechanics of static and low-velocity kinetic friction. Adv Chem Phys 2003:187–272. https://doi.org/10.1002/0471428019.ch5.
[67] Uygunoğlu T, Brostow W, Gunes I, Uygunoğlu T, Brostow W, Gunes I. Wear and friction of composites of an epoxy with boron containing wastes. Polímeros 2015;25:271–6. https://doi.org/10.1590/0104-1428.1780.
[68] Spikes H. Stress-augmented thermal activation: tribology feels the force. Friction 2018;6:1–31. https://doi.org/10.1007/s40544-018-0201-2.
[69] Aita Y, Asanuma N, Takahashi A, Mayama H, Nonomura Y. Nonlinear friction dynamics on polymer surface under accelerated movement. AIP Adv 2017;7:45005. https://doi.org/10.1063/1.4979883.
[70] Kado N, Tadokoro C, Nakano K. Kinetic friction coefficient measured in tribotesting: influence of frictional vibration. Tribol Online 2014;9:63–70. https://doi.org/10.2474/trol.9.63.
[71] Adams MJ, Johnson SA, Lefèvre P, Lévesque V, Hayward V, André T, et al. Finger pad friction and its role in grip and touch. J R Soc Interface 2013;10:20120467. https://doi.org/10.1098/rsif.2012.0467.
[72] Kim DE, Suh NP. On microscopic mechanisms of friction and wear. Wear 1991;149:199–208. https://doi.org/10.1016/0043-1648(91)90373-3.
[73] Lafaye S, Gauthier C, Schirrer R. Analysis of the apparent friction of polymeric surfaces. J Mater Sci 2006;41:6441–52. https://doi.org/10.1007/s10853-006-0710-7.
[74] Sinha SK. Handbook of polymer tribology. WORLD SCIENTIFIC; 2018. https://doi.org/10.1142/9789813227798_fmatter.
[75] Kozuka R. Studded tire wear - comparison between British Pendulum and Pin on disc testing. KTH Royal Institute of Technology in Stockholm; 2017.
[76] Adams GG, Müftü S, Azhar NM. A scale-dependent model for multi-asperity contact and friction. J Tribol 2003;125:700–8.
[77] Gao Z, Zhang W, Gao Y. Scale dependence of interface dislocation storage governing the frictional sliding of single asperities. Model Simul Mater Sci Eng 2016;24:065010https://doi.org/10.1088/0965-0393/24/6/065010.
[78] HJ A, Kyung–Suk K. Scale effects in friction of single–asperity contacts. I. From concurrent slip to single–dislocation–assisted slip. Proc R Soc London Ser A Math Phys Eng Sci 1999;455:3363–84. https://doi.org/10.1098/rspa.1999.0455.
[79] Pastewka L, Robbins MO. Contact between rough surfaces and a criterion for macroscopic adhesion. Proc Natl Acad Sci U S A 2014;111:3298–303. https://doi.org/10.1073/pnas.1320846111.

2019-08-15

Study of the mechanism of friction on functionally active tribological Polyvinyl þÿ C h l o r i d e (P V C) A g g r e g a t e c

Giannoukos, Konstantinos

Elsevier

Giannoukos K, Salonitis K. (2020) Study of the mechanism of friction on functionally active þÿ t r i b o l o g i c a l P o l y v i n y l C h l o r i d e (P V C) A g g r e g a t e c o m p o s i t e s u r f a c e s . T Volume 141, January 2020, Article number 105906

https://doi.org/10.1016/j.triboint.2019.105906